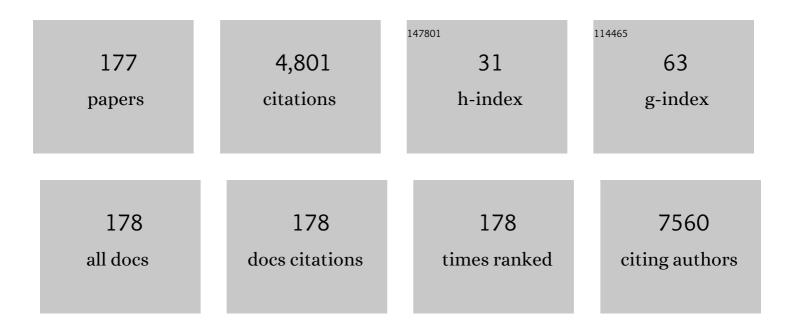
List of Publications by Year in descending order

Source: https://exaly.com/author-pdf/434911/publications.pdf Version: 2024-02-01



#	Article	IF	CITATIONS
1	Quantitative Assessment of Myocardial Ischemia With Positron Emission Tomography. Journal of Thoracic Imaging, 2023, 38, 247-259.	1.5	1
2	Algorithmic Prediction of Delayed Radiology Turn-Around-Time during Non-Business Hours. Academic Radiology, 2022, 29, e82-e90.	2.5	1
3	Data Management and Network Architecture Effect on Performance Variability in Direct Attenuation Correction via Deep Learning for Cardiac SPECT: A Feasibility Study. IEEE Transactions on Radiation and Plasma Medical Sciences, 2022, 6, 755-765.	3.7	0
4	Dosimetry in radionuclide therapy: the clinical role of measuring radiation dose. Lancet Oncology, The, 2022, 23, e75-e87.	10.7	26
5	Clinical language search algorithm from free-text: facilitating appropriate imaging. BMC Medical Imaging, 2022, 22, 18.	2.7	3
6	Incorporating Radiomics into Machine Learning Models to Predict Outcomes of Neuroblastoma. Journal of Digital Imaging, 2022, 35, 605-612.	2.9	12
7	First-in-human immunoPET imaging of HIV-1 infection using 89Zr-labeled VRC01 broadly neutralizing antibody. Nature Communications, 2022, 13, 1219.	12.8	20
8	Standardization of mineral density maps of physiologic and pathologic biominerals in humans using cone-beam CT and micro CT. Dental Materials, 2022, , .	3.5	0
9	Prediction of future healthcare expenses of patients from chest radiographs using deep learning: a pilot study. Scientific Reports, 2022, 12, 8344.	3.3	4
10	Application of a Domain-specific BERT for Detection of Speech Recognition Errors in Radiology Reports. Radiology: Artificial Intelligence, 2022, 4, .	5.8	7
11	Imaging joint infections using D-methyl-11C-methionine PET/MRI: initial experience in humans. European Journal of Nuclear Medicine and Molecular Imaging, 2022, 49, 3761-3771.	6.4	16
12	CUB Domain-Containing Protein 1 (CDCP1) Is a Target for Radioligand Therapy in Castration-Resistant Prostate Cancer, including PSMA Null Disease. Clinical Cancer Research, 2022, 28, 3066-3075.	7.0	10
13	An Analytical Algorithm for Tensor Tomography From Projections Acquired About Three Axes. IEEE Transactions on Medical Imaging, 2022, 41, 3454-3472.	8.9	3
14	Ferronostics: Measuring Tumoral Ferrous Iron with PET to Predict Sensitivity to Iron-Targeted Cancer Therapies. Journal of Nuclear Medicine, 2021, 62, jnumed.120.252460.	5.0	21
15	<sup>124</sup> I-MIBG PET/CT to Monitor Metastatic Disease in Children with Relapsed Neuroblastoma. Journal of Nuclear Medicine, 2021, 62, 43-47.	5.0	31
16	MR-Based Attenuation Correction for Brain PET Using 3-D Cycle-Consistent Adversarial Network. IEEE Transactions on Radiation and Plasma Medical Sciences, 2021, 5, 185-192.	3.7	22
17	Assessment of late-term progression of cardiac allograft vasculopathy in patients with orthotopic heart transplantation using quantitative cardiac 82Rb PET. International Journal of Cardiovascular Imaging, 2021, 37, 1461-1472.	1.5	2
18	Overcoming Barriers to Radiopharmaceutical Therapy (RPT): An Overview From the NRG-NCI Working Group on Dosimetry of Radiopharmaceutical Therapy. International Journal of Radiation Oncology Biology Physics, 2021, 109, 905-912.	0.8	13

#	Article	IF	CITATIONS
19	Molecular Imaging of Prostate Cancer Targeting CD46 Using ImmunoPET. Clinical Cancer Research, 2021, 27, 1305-1315.	7.0	18
20	Domain specific word embeddings for natural language processing in radiology. Journal of Biomedical Informatics, 2021, 113, 103665.	4.3	14
21	The Synthesis and Structural Requirements for Measuring Glucocorticoid Receptor Expression In Vivo with (±)- <sup>11</sup> C-YJH08 PET. Journal of Nuclear Medicine, 2021, 62, 723-731.	5.0	2
22	Direct Attenuation Correction Using Deep Learning for Cardiac SPECT: A Feasibility Study. Journal of Nuclear Medicine, 2021, 62, 1645-1652.	5.0	34
23	Direct image-based attenuation correction using conditional generative adversarial network for SPECT myocardial perfusion imaging. , 2021, 11600, .		10
24	CT-less Direct Correction of Attenuation and Scatter in the Image Space Using Deep Learning for Whole-Body FDG PET: Potential Benefits and Pitfalls. Radiology: Artificial Intelligence, 2021, 3, e200137.	5.8	28
25	Evaluation of a variableâ€aperture fullâ€ring SPECT system using largeâ€area pixelated CZT modules: A simulation study for brain SPECT applications. Medical Physics, 2021, 48, 2301-2314.	3.0	2
26	Mask-Guided Convolutional Neural Network for Breast Tumor Prognostic Outcome Prediction on 3D DCE-MR Images. Journal of Digital Imaging, 2021, 34, 630-636.	2.9	4
27	High precision localization of pulmonary nodules on chest CT utilizing axial slice number labels. BMC Medical Imaging, 2021, 21, 66.	2.7	2
28	Novel Methodology for Measuring Regional Myocardial Efficiency. IEEE Transactions on Medical Imaging, 2021, 40, 1711-1725.	8.9	2
29	Development and web deployment of an automated neuroradiology MRI protocoling tool with natural language processing. BMC Medical Informatics and Decision Making, 2021, 21, 213.	3.0	2
30	Gene therapy for aromatic L-amino acid decarboxylase deficiency by MR-guided direct delivery of AAV2-AADC to midbrain dopaminergic neurons. Nature Communications, 2021, 12, 4251.	12.8	83
31	Tomography of darkâ€field scatter including singleâ€exposure Moiré fringe analysis with Xâ€ray biprism interferometry—A simulation study. Medical Physics, 2021, 48, 6293-6311.	3.0	2
32	Xâ€ray biâ€prism interferometry—A design study of proposed novel hardware. Medical Physics, 2021, 48, 6508-6523.	3.0	1
33	Brown adipocyte ATF4 activation improves thermoregulation and systemic metabolism. Cell Reports, 2021, 36, 109742.	6.4	15
34	Maximizing the use of batch production of 18F-FDOPA for imaging of brain tumors to increase availability of hybrid PET/MR imaging in clinical setting. Neuro-Oncology Practice, 2021, 8, 91-97.	1.6	1
35	Functional Adaptation of LPSâ€affected Dentoalveolar Fibrous Joints in Rats. Journal of Periodontal Research, 2021, , .	2.7	1
36	PET imaging of glucose and fatty acid metabolism for NAFLD patients. Journal of Nuclear Cardiology, 2020, 27, 1689-1697.	2.1	5

#	Article	IF	CITATIONS
37	PET/CT Imaging of Human TNFα Using [89Zr]Certolizumab Pegol in a Transgenic Preclinical Model of Rheumatoid Arthritis. Molecular Imaging and Biology, 2020, 22, 105-114.	2.6	17
38	Quantitative and Qualitative Improvement of Low-Count [68Ga]Citrate and [90Y]Microspheres PET Image Reconstructions Using Block Sequential Regularized Expectation Maximization Algorithm. Molecular Imaging and Biology, 2020, 22, 208-216.	2.6	16
39	High Enantiomeric Excess In-Loop Synthesis of <scp>d</scp> -[methyl- <sup>11</sup> C]Methionine for Use as a Diagnostic Positron Emission Tomography Radiotracer in Bacterial Infection. ACS Infectious Diseases, 2020, 6, 43-49.	3.8	31
40	Improved diagnostic confidence and accuracy of pediatric elbow fractures with digital tomosynthesis. Pediatric Radiology, 2020, 50, 363-370.	2.0	2
41	An Analysis of Isoclonal Antibody Formats Suggests a Role for Measuring PD-L1 with Low Molecular Weight PET Radiotracers. Molecular Imaging and Biology, 2020, 22, 1553-1561.	2.6	11
42	An Open-Source, Vender Agnostic Hardware and Software Pipeline for Integration of Artificial Intelligence in Radiology Workflow. Journal of Digital Imaging, 2020, 33, 1041-1046.	2.9	24
43	Quantitative <sup>99m</sup> Tc Labeling Kit for HYNIC-Conjugated Single Chain Antibody Fragments Targeting Malignant Mesothelioma. Bioconjugate Chemistry, 2020, 31, 1750-1755.	3.6	2
44	Artificial Intelligence Pipeline for Risk Prediction in Cardiovascular Imaging. Circulation: Cardiovascular Imaging, 2020, 13, e010427.	2.6	1
45	Theranostic Targeting of CUB Domain Containing Protein 1 (CDCP1) in Pancreatic Cancer. Clinical Cancer Research, 2020, 26, 3608-3615.	7.0	24
46	Beneficial Effects of Melatonin on Apolipoprotein-E Knockout Mice by Morphological and 18F-FDG PET/CT Assessments. International Journal of Molecular Sciences, 2020, 21, 2920.	4.1	3
47	A Novel Radioligand Reveals Tissue Specific Pharmacological Modulation of Glucocorticoid Receptor Expression with Positron Emission Tomography. ACS Chemical Biology, 2020, 15, 1381-1391.	3.4	4
48	Preclinical SPECT and SPECT-CT in Oncology. Recent Results in Cancer Research, 2020, 216, 359-404.	1.8	1
49	Collimatorless Scintigraphy for Imaging Extremely Low Activity Targeted Alpha Therapy (TAT) with Weighted Robust Least Squares (WRLS). Lecture Notes in Computer Science, 2020, 12267, 803-811.	1.3	3
50	Evaluation of primary breast cancers using dedicated breast PET and whole-body PET. Scientific Reports, 2020, 10, 21930.	3.3	11
51	Development of <sup>64</sup> Cu-NOTA-Trastuzumab for HER2 Targeting: A Radiopharmaceutical with Improved Pharmacokinetics for Human Studies. Journal of Nuclear Medicine, 2019, 60, 26-33.	5.0	47
52	Slowed gastric emptying and improved oral glucose tolerance produced by a nanomolarâ€potency inhibitor of calciumâ€activated chloride channel TMEM16A. FASEB Journal, 2019, 33, 11247-11257.	0.5	14
53	Quantitative [ <sup>18</sup> F]-Naf-PET-MRI Analysis for the Evaluation of Dynamic Bone Turnover in a Patient with Facetogenic Low Back Pain. Journal of Visualized Experiments, 2019, , .	0.3	0
54	Initial experience of dedicated breast PET imaging of ER+ breast cancers using [F-18]fluoroestradiol. Npj Breast Cancer, 2019, 5, 12.	5.2	19

#	Article	IF	CITATIONS
55	Automatic Labeling of Special Diagnostic Mammography Views from Images and DICOM Headers. Journal of Digital Imaging, 2019, 32, 228-233.	2.9	6
56	Quantitative Imaging of Alpha-Emitting Therapeutic Radiopharmaceuticals. Nuclear Medicine and Molecular Imaging, 2019, 53, 182-188.	1.0	21
57	Joint correction of attenuation and scatter in image space using deep convolutional neural networks for dedicated brain <sup>18</sup> F-FDG PET. Physics in Medicine and Biology, 2019, 64, 075019.	3.0	65
58	Technical Note: Simplified and practical pretherapy tumor dosimetry — AÂfeasibility study for 131 l―MIBG therapy of neuroblastoma using 124 l―MIBG PET / CT. Medical Physics, 2019, 46, 2477-2486.	3.0	15
59	Parameters Estimation Directly from Sinograms with Neural Networks. , 2019, , .		2
60	Iterative PET Image Reconstruction Using Convolutional Neural Network Representation. IEEE Transactions on Medical Imaging, 2019, 38, 675-685.	8.9	188
61	A Deep Learning Model to Predict a Diagnosis of Alzheimer Disease by Using <sup>18</sup> F-FDG PET of the Brain. Radiology, 2019, 290, 456-464.	7.3	413
62	Phase I Study of CTT1057, an 18F-Labeled Imaging Agent with Phosphoramidate Core Targeting Prostate-Specific Membrane Antigen in Prostate Cancer. Journal of Nuclear Medicine, 2019, 60, 910-916.	5.0	35
63	Time of flight PET reconstruction using nonuniform update for regional recovery uniformity. Medical Physics, 2019, 46, 649-664.	3.0	2
64	A combined static-dynamic single-dose imaging protocol to compare quantitative dynamic SPECT with static conventional SPECT. Journal of Nuclear Cardiology, 2019, 26, 763-771.	2.1	8
65	Dynamic cardiac PET imaging: Technological improvements advancing future cardiac health. Journal of Nuclear Cardiology, 2019, 26, 1292-1297.	2.1	5
66	EMnet: an unrolled deep neural network for PET image reconstruction. , 2019, , .		19
67	MAPEM-Net: an unrolled neural network for Fully 3D PET image reconstruction. , 2019, , .		21
68	Multiresolution spatiotemporal mechanical model of the heart as a prior to constrain the solution for 4D models of the heart. , 2019, 11072, .		2
69	Zero-Echo-Time and Dixon Deep Pseudo-CT (ZeDD CT): Direct Generation of Pseudo-CT Images for Pelvic PET/MRI Attenuation Correction Using Deep Convolutional Neural Networks with Multiparametric MRI. Journal of Nuclear Medicine, 2018, 59, 852-858.	5.0	206
70	Quantitative and Visual Assessments toward Potential Sub-mSv or Ultrafast FDG PET Using High-Sensitivity TOF PET in PET/MRI. Molecular Imaging and Biology, 2018, 20, 492-500.	2.6	12
71	Direct 6D List-Mode Maximum-Likelihood Expectation-Maximization Reconstruction for Dynamic Cardiac SPECT. , 2018, , .		0
72	Targeting CD46 for both adenocarcinoma and neuroendocrine prostate cancer. JCI Insight, 2018, 3, .	5.0	43

#	Article	IF	CITATIONS
73	Attenuation correction for brain PET imaging using deep neural network based on Dixon and ZTE MR images. Physics in Medicine and Biology, 2018, 63, 125011.	3.0	97
74	Quantification of <sup>89</sup> Zrâ€ŀron oxide nanoparticle biodistribution using PETâ€MR and ultrashort TE sequences. Journal of Magnetic Resonance Imaging, 2018, 48, 1717-1720.	3.4	2
75	Vascular Cell Adhesion Molecule-Targeted MS2 Viral Capsids for the Detection of Early-Stage Atherosclerotic Plaques. Bioconjugate Chemistry, 2018, 29, 2526-2530.	3.6	22
76	Comparison of sparse domain approaches for 4D <scp>SPECT</scp> dynamic image reconstruction. Medical Physics, 2018, 45, 4493-4509.	3.0	2
77	Exploration of PET and MRI radiomic features for decoding breast cancer phenotypes and prognosis. Npj Breast Cancer, 2018, 4, 24.	5.2	79
78	Developing an efficient phase-matched attenuation correction method for quiescent period PET in abdominal PET/MRI. Physics in Medicine and Biology, 2018, 63, 185002.	3.0	5
79	Feasibility of myocardial PET imaging using a benzylguanidine analog: meta-(3-[18F]fluoropropyl)benzylguanidine ([18F]mFPBG). Nuclear Medicine and Biology, 2018, 61, 63-70.	0.6	4
80	Targeting iron metabolism in high-grade glioma with 68Ga-citrate PET/MR. JCI Insight, 2018, 3, .	5.0	26
81	Measurement of absolute myocardial blood flow in humans using dynamic cardiac SPECT and 99mTc-tetrofosmin: Method and validation. Journal of Nuclear Cardiology, 2017, 24, 268-277.	2.1	40
82	Technical Note: Fast respiratory motion estimation using sorted singles without unlist processing: A feasibility study. Medical Physics, 2017, 44, 1632-1637.	3.0	6
83	Dedicated Breast Positron Emission Tomography for the Evaluation of Early Response to Neoadjuvant Chemotherapy in Breast Cancer. Clinical Breast Cancer, 2017, 17, e155-e159.	2.4	13
84	Hybrid <scp>ZTE</scp> /Dixon <scp>MR</scp> â€based attenuation correction for quantitative uptake estimation of pelvic lesions in <scp>PET</scp> / <scp>MRI</scp> . Medical Physics, 2017, 44, 902-913.	3.0	73
85	Noninvasive PET quantitative myocardial blood flow with regadenoson for assessing cardiac allograft vasculopathy in orthotopic heart transplantation patients. Journal of Nuclear Cardiology, 2017, 24, 1134-1144.	2.1	12
86	Quantitative Evaluation of Atlas-based Attenuation Correction for Brain PET in an Integrated Time-of-Flight PET/MR Imaging System. Radiology, 2017, 284, 169-179.	7.3	19
87	11C-L-methyl methionine dynamic PET/CT of skeletal muscle: response to protein supplementation compared to L-[ring 13C6] phenylalanine infusion with serial muscle biopsy. Annals of Nuclear Medicine, 2017, 31, 295-303.	2.2	2
88	Evaluation of Sinus/Edge-Corrected Zero-Echo-Time–Based Attenuation Correction in Brain PET/MRI. Journal of Nuclear Medicine, 2017, 58, 1873-1879.	5.0	40
89	<i>MET</i> Exon 14 Mutation Encodes an Actionable Therapeutic Target in Lung Adenocarcinoma. Cancer Research, 2017, 77, 4498-4505.	0.9	57
90	Longitudinal Evaluation of Myocardial Fatty Acid and Glucose Metabolism in Fasted and Nonfasted Spontaneously Hypertensive Rats Using MicroPET/CT. Molecular Imaging, 2017, 16, 153601211772455.	1.4	6

#	Article	IF	CITATIONS
91	Imaging Hepatocellular Carcinoma With <sup>68</sup> Ga-Citrate PET: First Clinical Experience. Molecular Imaging, 2017, 16, 153601211772325.	1.4	6
92	[ <sup>18</sup> F]-Sodium Fluoride PET MR–Based Localization and Quantification of Bone Turnover as a Biomarker for Facet Joint–Induced Disability. American Journal of Neuroradiology, 2017, 38, 2028-2031.	2.4	13
93	Effect of Time-of-Flight and Regularized Reconstructions on Quantitative Measurements and Qualitative Assessments in Newly Diagnosed Prostate Cancer With <sup>18</sup> F-Fluorocholine Dual Time Point PET/MRI. Molecular Imaging, 2017, 16, 153601211773670.	1.4	1
94	18F Fluorocholine Dynamic Time-of-Flight PET/MR Imaging in Patients with Newly Diagnosed Intermediate- to High-Risk Prostate Cancer: Initial Clinical-Pathologic Comparisons. Radiology, 2017, 282, 429-436.	7.3	15
95	Tensor Tomography of Dark Field Scatter using X-ray Interferometry with Bi-prisms. , 2017, 2017, .		2
96	First-in-human phase 1 PET study of CTT1057, a novel <sup>18</sup> F-labeled imaging agent targeting prostate specific membrane antigen (PSMA) in prostate cancer Journal of Clinical Oncology, 2017, 35, e16562-e16562.	1.6	1
97	A compact energy-independent CZT-based gamma camera. , 2017, , .		0
98	Sparse domain approaches in dynamic SPECT imaging with high-performance computing. American Journal of Nuclear Medicine and Molecular Imaging, 2017, 7, 283-294.	1.0	1
99	Penalized MLAA with spatially-encoded anatomic prior in TOF PET/MR. , 2016, , .		1
100	A Feasibility Study Showing [68Ga]Citrate PET Detects Prostate Cancer. Molecular Imaging and Biology, 2016, 18, 946-951.	2.6	33
101	Biodistribution of Antibody-MS2 Viral Capsid Conjugates in Breast Cancer Models. Molecular Pharmaceutics, 2016, 13, 3764-3772.	4.6	50
102	Imaging Bone–Cartilage Interactions in Osteoarthritis Using [ <sup>18</sup> F]-NaF PET-MRI. Molecular Imaging, 2016, 15, 153601211668359.	1.4	50
103	Ictal lack of binding to brain parenchyma suggests integrity of the blood–brain barrier for <sup>11</sup> C-dihydroergotamine during glyceryl trinitrate-induced migraine. Brain, 2016, 139, 1994-2001.	7.6	66
104	[11C]acetate PET Imaging is not Always Associated with Increased Lipogenesis in Hepatocellular Carcinoma in Mice. Molecular Imaging and Biology, 2016, 18, 360-367.	2.6	11
105	Sentinel lymph node imaging guided IMRT for prostate cancer: Individualized pelvic radiation therapy versus RTOG guidelines. Advances in Radiation Oncology, 2016, 1, 51-58.	1.2	Ο
106	An energy-optimized collimator design for a CZT-based SPECT camera. Nuclear Instruments and Methods in Physics Research, Section A: Accelerators, Spectrometers, Detectors and Associated Equipment, 2016, 806, 330-339.	1.6	8
107	Quantitative analysis of hypertrophic myocardium using diffusion tensor magnetic resonance imaging. Journal of Medical Imaging, 2016, 3, 1.	1.5	12
108	Abstract 2790: Sensitizing the hypoxic tumor microenvironment with OMX, a breakthrough oxygen delivery protein: From protein engineering to clinical trial. , 2016, , .		0

#	Article	IF	CITATIONS
109	A simulation study comparing different pixel sizes of CZT detectors combined with pitch-matched collimators for SPECT imaging. , 2015, , .		0
110	Assessing Biological Response to Bevacizumab Using 18F-Fluoromisonidazole PET/MR Imaging in a Patient with Recurrent Anaplastic Astrocytoma. Case Reports in Radiology, 2015, 2015, 1-4.	0.3	16
111	Image reconstruction in higher dimensions: myocardial perfusion imaging of tracer dynamics with cardiac motion due to deformation and respiration. Physics in Medicine and Biology, 2015, 60, 8275-8301.	3.0	10
112	Bone Remodeling after MR Imaging–guided High-Intensity Focused Ultrasound Ablation: Evaluation with MR Imaging, CT, Na18F-PET, and Histopathologic Examination in a Swine Model. Radiology, 2015, 274, 387-394.	7.3	15
113	Differential Requirements for elF4E Dose in Normal Development and Cancer. Cell, 2015, 162, 59-71.	28.9	283
114	Patient-Specific Dosimetry Using Pretherapy [124I]m-iodobenzylguanidine ([124I]mIBG) Dynamic PET/CT Imaging Before [131I]mIBG Targeted Radionuclide Therapy for Neuroblastoma. Molecular Imaging and Biology, 2015, 17, 284-294.	2.6	67
115	Multipinhole collimator with 20 apertures for a brain SPECT application. Medical Physics, 2014, 41, 112501.	3.0	15
116	Improved Trabecular Bone Structure of 20-Month-Old Male Spontaneously Hypertensive Rats. Calcified Tissue International, 2014, 95, 282-291.	3.1	8
117	<em>In situ</em> Compressive Loading and Correlative Noninvasive Imaging of the Bone-periodontal Ligament-tooth Fibrous Joint. Journal of Visualized Experiments, 2014, , .	0.3	12
118	The effect of magnetic field on positron range and spatial resolution in an integrated whole-body time-of-flight PET/MRI system. , 2014, 2014, .		7
119	Parallelization of iterative reconstruction algorithms in multiple modalities. , 2014, 2014, .		2
120	Handling Big Data in medical imaging: Iterative reconstruction with large-scale automated parallel computation. , 2014, 2014, .		1
121	Quantitative signature of coronary steal in a patient with occluded coronary arteries supported by collateral circulation using dynamic SPECT. , 2014, 2014, .		1
122	Dual-Modality Preclinical SPECT/CT Instrumentation. , 2014, , 351-365.		0
123	Design studies of a CZT-based detector combined with a pixel-geometry-matching collimator for SPECT imaging. , 2013, 2013, 1-4.		1
124	Preclinical SPECT and SPECT/CT. Recent Results in Cancer Research, 2013, 187, 193-220.	1.8	1
125	Longitudinal Evaluation of Left Ventricular Substrate Metabolism, Perfusion, and Dysfunction in the Spontaneously Hypertensive Rat Model of Hypertrophy Using Small-Animal PET/CT Imaging. Journal of Nuclear Medicine, 2013, 54, 1938-1945.	5.0	30
126	Design and performance evaluation of a 20-aperture multipinhole collimator for myocardial perfusion imaging applications. Physics in Medicine and Biology, 2013, 58, 7209-7226.	3.0	17

#	ARTICLE	IF	CITATIONS
127	Myocardial blood flow measurement with a conventional dual-head SPECT/CT with spatiotemporal iterative reconstructions - a clinical feasibility study. American Journal of Nuclear Medicine and Molecular Imaging, 2013, 4, 53-9.	1.0	8
128	A dynamic single photon emission computed tomography myocardial perfusion imaging protocol using a 4D spatiotemporal iterative reconstruction. , 2012, , .		1
129	Energy response of a room-temperature cadmium telluride (CdTe) photon-counting detector for simultaneous and sequential CT and SPECT. , 2012, , .		0
130	Combining dynamic and ECG-gated 82Rb-PET for practical implementation in the clinic. Nuclear Medicine Communications, 2012, 33, 4-13.	1.1	1
131	The impact of audio-visual biofeedback on 4D PET images: Results of a phantom study. Medical Physics, 2012, 39, 1046-1057.	3.0	18
132	Tumor Dosimetry Using [124I]m-iodobenzylguanidine MicroPET/CT for [131I]m-iodobenzylguanidine Treatment of Neuroblastoma in a Murine Xenograft Model. Molecular Imaging and Biology, 2012, 14, 735-742.	2.6	42
133	Intravenous Vasopressin for the Prevention of Nontarget Gastrointestinal Embolization during Liver-directed Cancer Treatment: Experimental Study in a Porcine Model. Journal of Vascular and Interventional Radiology, 2012, 23, 1505-1512.	0.5	4
134	The Metabolic Profile of Tumors Depends on Both the Responsible Genetic Lesion and Tissue Type. Cell Metabolism, 2012, 15, 157-170.	16.2	553
135	Functional Imaging for Prostate Cancer: Therapeutic Implications. Seminars in Nuclear Medicine, 2012, 42, 328-342.	4.6	18
136	Reconstruction of gated dynamic cardiac SPECT data using spatiotemporal basis functions. , 2012, , .		2
137	Combined SPECT and Multidetector CT for Prostate Cancer Evaluations. American Journal of Nuclear Medicine and Molecular Imaging, 2012, 2, 48-54.	1.0	17
138	Assessing cervical dislocation as a humane euthanasia method in mice. Journal of the American Association for Laboratory Animal Science, 2012, 51, 352-6.	1.2	43
139	Depth-of-Interaction Compensation Using a Focused-Cut Scintillator for a Pinhole Gamma Camera. IEEE Transactions on Nuclear Science, 2011, 58, 634-638.	2.0	4
140	Temperature Dependent Operation of PSAPD-Based Compact Gamma Camera for SPECT Imaging. IEEE Transactions on Nuclear Science, 2011, 58, 2169-2174.	2.0	8
141	Compact CdZnTe-based gamma camera for prostate cancer imaging. , 2011, , .		3
142	Ultrafast multipinhole single photon emission computed tomography iterative reconstruction using CUDA. , 2011, , .		5
143	The effect of internalizing human single chain antibody fragment on liposome targeting to epithelioid and sarcomatoid mesothelioma. Biomaterials, 2011, 32, 2605-2613.	11.4	45
144	Novel Human Single Chain Antibody Fragments That Are Rapidly Internalizing Effectively Target Epithelioid and Sarcomatoid Mesotheliomas. Cancer Research, 2011, 71, 2428-2432.	0.9	18

#	Article	IF	CITATIONS
145	Phantom measurements and simulations of cardiac and brain studies using a multipinhole collimator with 20 apertures. , 2011, , .		1
146	Multi-material decomposition using low-current X-ray and a photon-counting CZT detector. , 2011, , 4735-4738.		0
147	Vorinostat Increases Expression of Functional Norepinephrine Transporter in Neuroblastoma <i>In Vitro</i> and <i>In Vivo</i> Model Systems. Clinical Cancer Research, 2011, 17, 2339-2349.	7.0	61
148	Mapping of Lymphatic Drainage from the Prostate Using Filtered <sup>99m</sup> Tc-Sulfur Nanocolloid and SPECT/CT. Journal of Nuclear Medicine, 2011, 52, 1068-1072.	5.0	19
149	A preclinical SPECT camera with depth-of-interaction compensation using a focused-cut scintillator. , 2011, , .		2
150	Patient-Specific Method of Generating Parametric Maps of Patlak Ki without Blood Sampling or Metabolite Correction: A Feasibility Study. International Journal of Molecular Imaging, 2011, 2011, 1-12.	1.3	9
151	Radiation dose estimation using preclinical imaging with â€metaiodobenzylguanidine (MIBG) PET. Medical Physics, 2010, 37, 4861-4867.	3.0	60
152	Selective activation of p53-mediated tumour suppression in high-grade tumours. Nature, 2010, 468, 567-571.	27.8	233
153	Experimental feasibility of multi-material decomposition imaging in small animal SPECT/CT system. , 2010, , .		0
154	SPECT dual-isotope myocardial perfusion imaging with a 20-pinhole collimator: A simulation study. , 2010, , .		1
155	Depth-of-interaction compensation using a focused-cut scintillator for a pinhole gamma camera. , 2010, , .		1
156	Targeting Prostate Cancer Cells In Vivo Using a Rapidly Internalizing Novel Human Single-Chain Antibody Fragment. Journal of Nuclear Medicine, 2010, 51, 427-432.	5.0	33
157	In Vivo Tumor Grading of Prostate Cancer Using Quantitative <sup>111</sup> In-Capromab Pendetide SPECT/CT. Journal of Nuclear Medicine, 2010, 51, 31-36.	5.0	29
158	Phantom Experiments on a PSAPD-Based Compact Gamma Camera With Submillimeter Spatial Resolution for Small Animal SPECT. IEEE Transactions on Nuclear Science, 2010, 57, 2518-2523.	2.0	6
159	Functional Imaging Combined with Multi-Detector CT: A Radionuclide Imaging Perspective. Current Medical Imaging, 2010, 6, 100-111.	0.8	2
160	Biodistributions of 177Lu- and 111In-Labeled 7E11 Antibodies to Prostate-Specific Membrane Antigen in Xenograft Model of Prostate Cancer and Potential Use of 111In-7E11 as a Pre-therapeutic Agent for 177Lu-7E11 Radioimmunotherapy. Molecular Imaging and Biology, 2009, 11, 159-166.	2.6	26
161	Technological Development and Advances in Single-Photon Emission Computed Tomography/Computed Tomography. Seminars in Nuclear Medicine, 2008, 38, 177-198.	4.6	172

162 Prostate-bladder phantom for radionuclide imaging research. , 2008, , .

#	Article	IF	CITATIONS
163	<i>In vivo</i> microCT imaging of rodent cerebral vasculature. Physics in Medicine and Biology, 2008, 53, N99-N107.	3.0	17
164	Nanoprobes for Medical Diagnosis: Current Status of Nanotechnology in Molecular Imaging. Current Nanoscience, 2008, 4, 17-29.	1.2	32
165	Quantitative accuracy of PET/CT for image-based kinetic analysis. Medical Physics, 2008, 35, 3086-3089.	3.0	10
166	Correcting tumour SUV for enhanced bone marrow uptake: retrospective 18F-FDG PET/CT studies. Nuclear Medicine Communications, 2008, 29, 359-366.	1.1	12
167	Quantification of SPECT and PET for Drug Development. Current Radiopharmaceuticals, 2008, 1, 17-21.	0.8	14
168	Rodent brain imaging with SPECT/CT. Medical Physics, 2007, 34, 1217-1220.	3.0	11
169	Quantitative accuracy of PET for image-based kinetic analysis. , 2007, , .		0
170	Partial-volume correction in PET: validation of an iterative postreconstruction method with phantom and patient data. Journal of Nuclear Medicine, 2007, 48, 802-10.	5.0	134
171	Rodent Brain Imaging with SPECT and CT. , 2006, , .		0
172	Progress in SPECT/CT Imaging of Prostate Cancer. Technology in Cancer Research and Treatment, 2006, 5, 329-336.	1.9	20
173	Calculation and validation of the use of effective attenuation coefficient for attenuation correction in In-111 SPECT. Medical Physics, 2005, 32, 3628-3635.	3.0	32
174	Improved prostate cancer imaging with SPECT/CT and MRI/MRSI. IEEE Transactions on Nuclear Science, 2005, 52, 1316-1320.	2.0	7
175	Correction of photon attenuation and collimator response for a body-contouring SPECT/CT imaging system. Journal of Nuclear Medicine, 2005, 46, 868-77.	5.0	42
176	Measurement of the μ decay spectrum with the ICARUS liquid Argon TPC. European Physical Journal C, 2004, 33, 233-241.	3.9	50
177	Monte Carlo Simulation and Reconstruction: Assessment of Myocardial Perfusion Imaging of Tracer Dynamics With Cardiac Motion Due to Deformation and Respiration Using Gamma Camera With Continuous Acquisition. Frontiers in Cardiovascular Medicine, 0, 9, .	2.4	1